

LA-UR-17-22948 (Accepted Manuscript)

# Incommensurate to commensurate antiferromagnetism in CeRhAl4Si2: An $^{27}\text{Al}$ NMR study

Sakai, Hironori  
Hattori, T  
Tokunaga, Y.  
Kambe, Shin  
Ghimire, N. J.  
Ronning, Filip  
Bauer, Eric Dietzgen  
Thompson, Joe David

Provided by the author(s) and the Los Alamos National Laboratory (2018-06-11).

**To be published in:** Physical Review B

**DOI to publisher's version:** 10.1103/PhysRevB.93.014402

**Permalink to record:** <http://permalink.lanl.gov/object/view?what=info:lanl-repo/lareport/LA-UR-17-22948>

**Disclaimer:**

Approved for public release. Los Alamos National Laboratory, an affirmative action/equal opportunity employer, is operated by the Los Alamos National Security, LLC for the National Nuclear Security Administration of the U.S. Department of Energy under contract DE-AC52-06NA25396. Los Alamos National Laboratory strongly supports academic freedom and a researcher's right to publish; as an institution, however, the Laboratory does not endorse the viewpoint of a publication or guarantee its technical correctness.

This is the accepted manuscript made available via CHORUS. The article has been published as:

## Incommensurate to commensurate antiferromagnetism in CeRhAl<sub>4</sub>Si<sub>2</sub>: An <sup>27</sup>Al NMR study

H. Sakai, T. Hattori, Y. Tokunaga, S. Kambe, N. J. Ghimire, F. Ronning, E. D. Bauer, and J. D. Thompson

Phys. Rev. B **93**, 014402 — Published 4 January 2016

DOI: [10.1103/PhysRevB.93.014402](https://doi.org/10.1103/PhysRevB.93.014402)

# Incommensurate to commensurate antiferromagnetism in CeRhAl<sub>4</sub>Si<sub>2</sub>: An <sup>27</sup>Al NMR Study

H. Sakai,\* T. Hattori, Y. Tokunaga, and S. Kambe

Advanced Science Research Center, Japan Atomic Energy Agency, Tokai, Ibaraki, 319-1195, Japan.

N. J. Ghimire,<sup>†</sup> F. Ronning, E. D. Bauer, and J. D. Thompson  
Los Alamos National Laboratory, Los Alamos, NM 87545, USA

<sup>27</sup>Al nuclear magnetic resonance (NMR) experiments have been performed on a single crystal of CeRhAl<sub>4</sub>Si<sub>2</sub>, which is an antiferromagnetic Kondo-lattice compound with successive antiferromagnetic transitions of  $T_{N1}=14$  K and  $T_{N2}=9$  K at zero external field. In the paramagnetic state, the Knight shifts, quadrupolar frequency, and asymmetric parameter of electrical field gradient on the Al sites have been determined, which have local orthorhombic symmetry. The transferred hyperfine coupling constants are also determined. Analysis of the NMR spectra indicates that a commensurate antiferromagnetic structure exists below  $T_{N2}$ , but an incommensurate modulation of antiferromagnetic moments is present in the antiferromagnetic state between  $T_{N1}$  and  $T_{N2}$ . The spin-lattice relaxation rate suggests that the 4f electrons behave as local moments at temperatures above  $T_{N1}$ .

PACS numbers: 75.20.Hr, 75.25.-j, 76.60.-k

## I. INTRODUCTION

In Ce-based intermetallic compounds, the competition between the Ruderman-Kittel-Kasuya-Yosida (RKKY) exchange interaction and the Kondo effect leads to a rich variety of physical phenomena, such as magnetic ordering, non-Fermi-liquid behavior, and unconventional superconductivity. Due to a delicate balance of competing interactions, various magnetic ground states emerge. Antiferromagnetic (AFM) phases are widely seen in heavy fermion systems, and are roughly classified into two groups, i.e., order of *f* moments and spin density wave (SDW) of itinerant *f* electrons. Representative materials are CeRhIn<sub>5</sub><sup>1</sup> and CeCu<sub>2</sub>Si<sub>2</sub><sup>2</sup>, both of which adjoin superconducting phases<sup>3,4</sup> near AFM quantum critical points. To understand the physical properties in such compounds, it is very important to investigate the magnetic structure and excitations of new magnetic systems with competing interactions.

A tetragonal compound CeRhAl<sub>4</sub>Si<sub>2</sub>, which is one of the series Ce $T_n$ Al<sub>2n+2</sub>Si<sub>2</sub> ( $T$ =Rh, Ir, Pt), has been reported as a new AFM Kondo lattice with successive AFM transitions of  $T_{N1}=14$  K and  $T_{N2}=9$  K at zero external field.<sup>5,6</sup> These Ce $T$ Al<sub>4</sub>Si<sub>2</sub> ( $T$ =Rh, Ir, Pt) materials crystallize in the tetragonal KCu<sub>4</sub>S<sub>3</sub>-type structure with space group *P4/mmm*, as displayed in Fig. 1(a) for CeRhAl<sub>4</sub>Si<sub>2</sub>. The Ce atoms that reside on 1*b* sites with atomic coordinates of (0, 0, 0.5) form a simple tetragonal lattice, and the Rh atoms occupy the 1*a* site at (0, 0, 0). Each metallic atom of Ce and Rh is surrounded by *p*-block Si and/or Al atoms, where the Si and Al atoms occupy 2*h* sites at (0.5, 0.5,  $z_{Si}$ ) and 4*i* sites at (0, 0.5,  $z_{Al}$ ), respectively, where  $z_{Si}=0.3546$  and  $z_{Al}=0.1719$  are obtained from powder neutron diffraction<sup>7</sup>. In this quaternary compound, the square lattices of Ce-Ce with  $a=4.22$  Å are well separated from each other along the *c*-axis of 8.01 Å. Due to the layered crystal structure, a quasi-two-

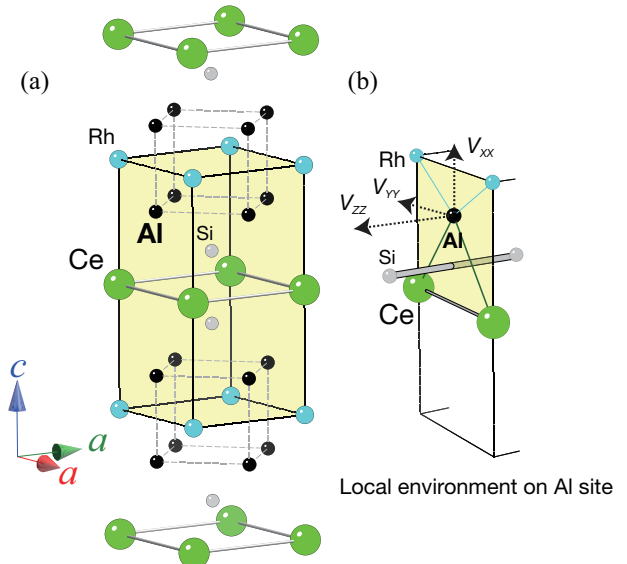


FIG. 1. (Color online) (a) Crystal structure of CeRhAl<sub>4</sub>Si<sub>2</sub>. The unit cell is shaded. To visualize the intervals between Ce planes, the structure is drawn in the range between the upper and lower Ce planes. (b) Local atomic environment of the Al site. The deduced principal axes of electrical field gradient on the Al site are also illustrated.

dimensional electronic structure might be expected. Indeed, density functional theory (DFT) calculations using the generalized gradient approximation (GGA) predict a quasi-two-dimensional character of the Fermi surface with a propensity for nesting in the *ab* plane as well as along the *c*-axis.<sup>5</sup> From magnetization measurements on CeRhAl<sub>4</sub>Si<sub>2</sub>, the effective moment in the paramagnetic (PM) state above about 200 K is close to the free ion value  $2.54 \mu_B$  of Ce<sup>3+</sup>, indicating localized 4*f* electrons. The estimated entropy via specific heat measurements suggests that the Kondo energy scale is comparable to

the RKKY interaction scale ( $T_K \sim T_N$ ), where the  $f$  electrons strongly hybridize with conduction electrons. Recent magnetization and specific heat experiments on CeRhAl<sub>4</sub>Si<sub>2</sub> have clarified the complex phase diagram of external field ( $H_0$ ) vs temperature, and proposed that the  $J = 5/2$  manifold is split into three doublets by the crystalline electric field (CEF), i.e., the ground state would be a  $\Gamma_7^{(1)}$  doublet, the first excited  $\Gamma_6$  doublet would lie at  $E_1 = 136$  K, and the second excited  $\Gamma_7^{(2)}$  doublet is estimated to be 342 K from the ground state.<sup>6</sup> Indeed, this CEF level scheme has been used to explain the *Ising*-anisotropy of magnetic susceptibility along the  $c$ -axis. Two AFM transitions at  $T_{N1}$  and  $T_{N2}$  are observed in specific heat, confirming long-range antiferromagnetism<sup>5,6</sup>. Powder neutron diffraction experiments<sup>7</sup> provide evidence for a simple AFM structure below  $T_{N2}$  with a propagation vector  $\mathbf{Q}_2 = (0, 0, 1/2)$ , where the Ce moments of  $\sim 1 \mu_B/\text{Ce}$  align ferromagnetically in the  $ab$ -plane and stack antiferromagnetically along the  $c$ -axis, although, the intermediate AFM structure between  $T_{N1}$  and  $T_{N2}$  could not be determined. Recently, the intermediate AFM structure has been determined by neutron diffraction on single crystals<sup>8</sup> to have an incommensurate wavevector of  $\mathbf{Q}_1 = (\delta, \delta, 1/2)$ , with a temperature dependent propagation and “locks in” to the commensurate AFM at  $T_{N1}$ . To account for their data, the authors propose a model of a spin-density wave order with the Ce moments modulated along the  $a$ -axis due to Fermi surface nesting.<sup>8</sup>

In general, NMR is a particularly useful tool for the microscopic investigation of the magnetism of materials, providing information about magnetic ordering that is complementary to other microscopic probes. In addition, NMR may also be used to probe magnetic dynamics. In this paper, we report a <sup>27</sup>Al NMR investigation on the new Kondo compound CeRhAl<sub>4</sub>Si<sub>2</sub>. We first investigated the hyperfine parameters in the paramagnetic state. To obtain the electric field gradient (EFG) parameters, we measured the angular dependence of the <sup>27</sup>Al NMR spectra. As shown in Fig. 1(b), because the local symmetry of Al sites is orthorhombic (2mm), such a directional measurement of NMR is important for assignment of the Al NMR lines. In the antiferromagnetically ordered states, a broadening of the NMR spectra has been observed, which is due to the development of internal fields at the ligand Al sites. Based on the analysis of the NMR spectra in the ordered state, an incommensurate magnetic structure in the intermediate state between  $T_{N1}$  and  $T_{N2}$  and a commensurate magnetic structure below  $T_{N2}$  are deduced. Finally, we present the relaxation rate data and anisotropy and discuss the nature of the 4f electrons in CeRhAl<sub>4</sub>Si<sub>2</sub>.

## II. EXPERIMENTAL

Single crystals of CeRhAl<sub>4</sub>Si<sub>2</sub> were grown from Al/Si flux.<sup>5</sup> The chemical composition and homogeneity of sin-

gle crystals were confirmed using a scanning electron microscope (SEM) with an energy dispersive x-ray spectrometer (EDS). Magnetization was measured using a SQUID magnetometer (Quantum Design Magnetic Property Measurement System) between 1.8 K and 350 K and in magnetic fields up to 60 kOe.

Several single crystals with a typical dimension of  $3 \times 2 \times 1 \text{ mm}^3$  were scanned for NMR purposes to check for identical Al NMR spectra. Finally we chose the thinnest piece with  $2 \times 2 \times 0.16 \text{ mm}^3$  to avoid twinned domains. The specimen was inserted into an rf excitation coil of copper and mounted on a two-axes goniometer installed in the NMR probe. In order to avoid overlap of <sup>63</sup>Cu and sample NMR signals, some <sup>27</sup>Al NMR spectra were taken with a silver coil instead of a copper coil. NMR measurements were carried out using a phase-coherent, pulsed spectrometer. External magnetic fields were applied using a homogeneous superconducting magnet specified for NMR. To form the nuclear spin echoes, 90°-180° conditions were used with a first pulse duration of 2-3  $\mu\text{sec}$ . The separation  $\tau$  between first and second pulses was typically 10-30  $\mu\text{sec}$ . In the ordered state, to confirm the spectral shapes, the echo intensities were corrected by the intensities taken at several  $\tau$  values. Frequency-swept spectra were measured by tuning the rf network at each frequency, of which steps were 25-50 kHz apart. To obtain the entire NMR spectrum, Fast-Fourier-Transform (FFT) spectra at the respective frequencies were overlapped.

Using conventional notation, the quadrupole frequency parameter is defined as  $\nu_Q \equiv \frac{3e^2 q Q}{2I(2I-1)\hbar}$ , where  $eQ$  is the nuclear quadrupolar moment,  $I$  is the nuclear spin quantum number, and  $eq \equiv V_{ZZ}$  is the principal component of the electric field gradient (EFG) tensor. Here,  $V_{ii}$  denotes the EFG tensor components in the principal coordinate system, such that  $|V_{XX}| \leq |V_{YY}| \leq |V_{ZZ}|$  for each ionic site. The EFG components satisfy LaPlace’s equation, i.e.,  $V_{XX} + V_{YY} + V_{ZZ} = 0$ . The EFG asymmetry parameter is defined as  $\eta \equiv \frac{|V_{YY} - V_{XX}|}{|V_{ZZ}|}$ . The nuclear quadrupolar moment is  $^{27}Q = 0.149 \times 10^{-24} \text{ cm}^2$ . The nuclear gyromagnetic ratio value is  $^{27}\gamma_N/2\pi = 1.1094 \text{ MHz/kOe}$ .

The nuclear spin-lattice relaxation time  $T_1$  was measured using the inversion-recovery method with a  $\pi$ -pulse. Values of  $T_1$  were obtained from fits to an appropriate relaxation function. The magnetization recovery ( $\{M(\infty) - M(t)\}/M(\infty)$ ) for the central and second satellite NMR transitions of the <sup>27</sup>Al ( $I = 5/2$ ) nuclei gave satisfactory fits to the single- $T_1$  functions:  $\frac{1}{35} \exp(-t/T_1) + \frac{8}{45} \exp(-6t/T_1) + \frac{50}{63} \exp(-15t/T_1)$  for the central transition, and  $\frac{1}{35} \exp(-t/T_1) + \frac{3}{14} \exp(-3t/T_1) + \frac{2}{5} \exp(-6t/T_1) + \frac{2}{7} \exp(-10t/T_1) + \frac{1}{14} \exp(-15t/T_1)$  for the second satellite transition, respectively.

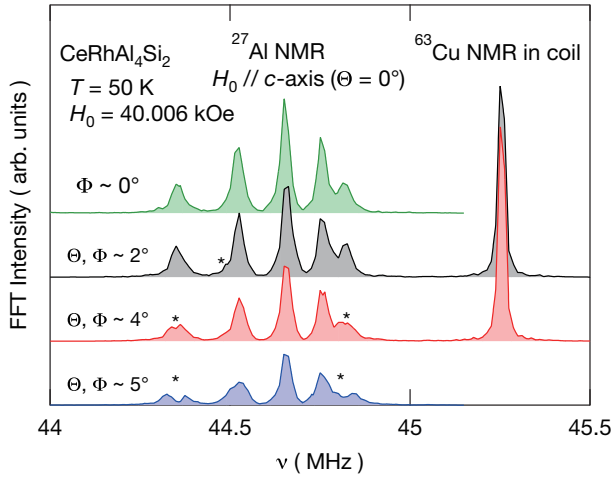


FIG. 2. (Color online)  $^{27}\text{Al}$  NMR spectra in a single crystal of  $\text{CeRhAl}_4\text{Si}_2$  at 50 K under external field of  $H_0 = 40.006$  kOe for  $H_0 \parallel c$ . The external field was calibrated by the resonance frequency of  $^{63}\text{Cu}$  NMR in the coil. Slightly misaligned spectra with  $\Theta$  and/or  $\Phi \sim 2^\circ, 4^\circ$ , and  $5^\circ$  are also shown. The asterisks (\*) indicate small NMR line splittings.

### III. RESULTS AND DISCUSSIONS

#### A. $^{27}\text{Al}$ NMR spectral assignment in the paramagnetic state

Figure 2 shows the  $^{27}\text{Al}$  NMR spectrum taken in the PM state at 50 K using a single crystal of  $\text{CeRhAl}_4\text{Si}_2$  in an external field  $H_0$  of 40.006 kOe along the  $c$  axis, which was established by tuning the sample orientation with a two-axes goniometer. The exact magnitude of the external field was determined by the frequency of  $^{63}\text{Cu}$  NMR in the rf coil, as shown in Fig. 2. Here, the polar angles  $\Theta$  and  $\Phi$  of the external field direction are defined relative to the  $c$ - and  $a$ -axes, respectively, of the crystal lattice.

In general, because the nuclear spin ( $I$ ) of  $^{27}\text{Al}$  with a natural abundance of 100% is  $5/2$ , one equivalent Al site gives five NMR lines if the site-symmetry is lower than cubic due to the nuclear quadrupolar interaction: one central ( $-1/2 \leftrightarrow 1/2$ ), two first satellite ( $-1/2 \leftrightarrow -3/2, 1/2 \leftrightarrow 3/2$ ), and two second satellite ( $-5/2 \leftrightarrow -3/2, 3/2 \leftrightarrow 5/2$ ) transitions. In the case of  $H_0 \parallel c$ , as shown in Fig. 2, five NMR lines appear at irregular intervals, which are due to the orthorhombic (non-axial) symmetry. In  $\text{CeRhAl}_4\text{Si}_2$ , by the site symmetry of  $2mm$  on the Al sites, the maximal principal EFG axis ( $V_{ZZ}$ ) should correspond to the  $a$  or  $c$  axis, and the minimal principal axis ( $V_{XX}$ ) should correspond to the alternative  $c$  or  $a$  axis. In the case of  $H_0 \parallel c$ , therefore, all the Al sites are equivalent. If the direction of the external field deviates from the  $c$ -axis, the  $^{27}\text{Al}$  NMR spectrum shows a slight line splitting of the satellite transitions, as indicated by asterisks in Fig. 2, because even a small misalignment makes the two Al sites inequivalent.

Moreover, if the direction of the external field is rotated in the  $a$ - $c$  plane from  $\Theta = 0^\circ$  to  $\Theta = 90^\circ$  keeping  $\Phi = 0^\circ$  fixed, as shown in Fig. 3, the five NMR lines for  $H_0 \parallel c$  split into two sets of five lines with increasing intervals between the respective satellite transitions for increasing  $\Theta$ , while the central transitions do not shift much. For  $H_0 \parallel a$ , a total of 10 lines for  $^{27}\text{Al}$  NMR is clearly observed. The minimal splitting in the case of  $H_0 \parallel c$  experimentally confirms that the  $c$ -component of EFG is minimal, i.e.,  $V_{XX}$  corresponds to the  $c$  axis, and consequently  $V_{ZZ}$  is along the  $a$ -axis, as shown in Fig. 1. If  $H_0 \parallel a$ , then  $H_0$  is parallel to  $V_{ZZ}$  on half of the Al sites, which are defined as Al( $a$ ) sites, but  $H_0$  is perpendicular to  $V_{ZZ}$  on the other half of the Al sites, defined as Al( $b$ ) sites.

The angular dependence of resonant frequencies can be reproduced by the following calculation. It is convenient to introduce the polar angles  $\theta$  and  $\phi$  for the local EFG coordinate on each Al site. In this procedure,  $\theta$  varies from  $90^\circ$  to  $0^\circ$  but  $\phi$  is fixed at  $0^\circ$  for the Al( $a$ ) sites, but  $\theta$  remains fixed at  $90^\circ$  and  $\phi$  varies from  $0^\circ$  to  $90^\circ$  for the Al( $b$ ) sites. In each of the Al sites, if the magnetic field is applied in the orientation of  $(\theta, \phi)$ , the nuclear Hamiltonian matrix consists of the Zeeman interaction including the Knight shift  $K$  and nuclear quadrupolar interaction. The former is

$$\mathcal{H}_Z = \gamma_N \hbar \{1 + K(\theta, \phi)\} \mathbf{I} \cdot \mathbf{H}_0, \quad (1)$$

and the latter is

$$\mathcal{H}_Q = \frac{h\nu_Q}{6} \left\{ 3I_z^2 - I(I+1) + \frac{\eta}{2}(I_+^2 + I_-^2) \right\}. \quad (2)$$

The resonant frequencies are numerically calculated by exact diagonalization of  $\mathcal{H}_Z + \mathcal{H}_Q$  for each orientation for the respective Al sites. If the diagonal terms of the Knight shift tensor are defined as  $K_a$ ,  $K_b$ , and  $K_c$  in the lattice frame,  $K(\theta, \phi)$  may be represented as  $K_c \sin^2 \theta + K_a \cos^2 \theta$  for the Al( $a$ ) sites, and  $K(\theta, \phi) = K_c \cos^2 \phi + K_b \sin^2 \phi$  for the Al( $b$ ) sites. The parameters to be determined are now Knight shifts  $K_a$ ,  $K_b$ ,  $K_c$ , and EFG parameters  $\nu_Q$ , and  $\eta$ . A least-squares fit to the data yields the values  $K_a = 0.0734\%$ ,  $K_b = 0.0978\%$ ,  $K_c = 0.516\%$ ,  $\nu_Q = 1.607$  MHz, and  $\eta = 0.856$ . Indeed, as shown in Fig. 4, the simulated curves using these parameters reproduce the resonant frequencies.

To check the validity of the obtained EFG parameters, the EFG on the Al sites of  $\text{LaRhAl}_4\text{Si}_2$  and  $\text{CeRhAl}_4\text{Si}_2$  has been computed based on a DFT electronic structure calculation<sup>5</sup> using the exchange correlation functional of Perdew-Burke-Ernzerhof<sup>9</sup> as implemented in the WIEN2K code<sup>10</sup>. Spin-orbit coupling was included in a second variational scheme without including additional “relativistic local orbitals”. In this case, the  $4f$  electrons of  $\text{CeRhAl}_4\text{Si}_2$  are treated as itinerant, but the La analogs would provide an estimate for the localized  $4f$  case. The calculated values are  $\nu_Q = 1.61$  MHz ( $V_{ZZ} = 2.98 \times 10^{21}$  V/m $^2$ ) with  $\eta = 0.78$  for  $\text{LaRhAl}_4\text{Si}_2$ ,

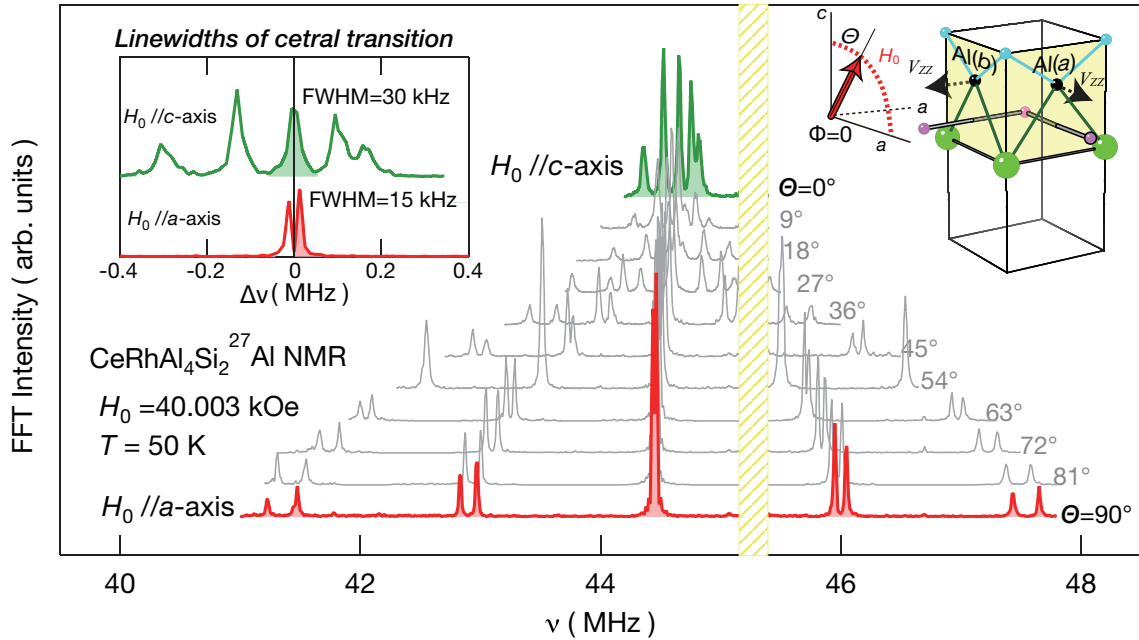


FIG. 3. (Color online) Magnetic field-angular dependence of the  $^{27}\text{Al}$  NMR spectrum at 50 K with an external field of 40.003 kOe rotated from  $\langle 001 \rangle$  to  $\langle 100 \rangle$  in the  $a$ - $c$  plane, as schematically illustrated in the right inset. In the left inset, the enlarged spectra in the relative frequency scale around central transition for  $H_0 \parallel c$ - and  $a$ -axis are shown for comparison of the line widths. The  $^{63}\text{Cu}$  NMR lines are masked by a shaded rectangle for clarity.

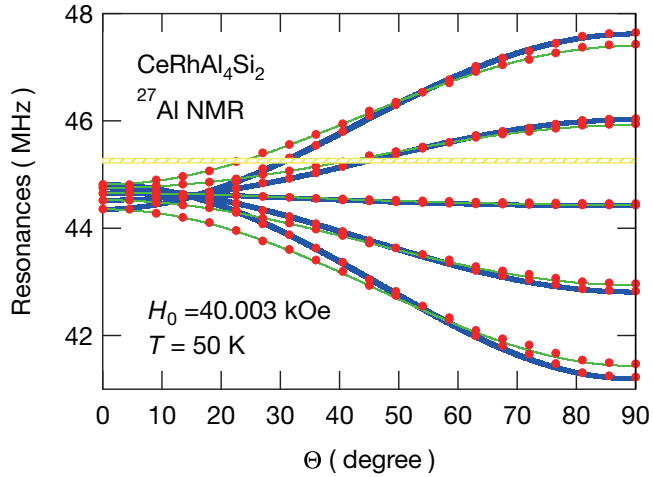


FIG. 4. (Color online) Magnetic field-angular dependence of the resonant frequencies at 50 K with an external field of 40.003 kOe applied from  $\langle 001 \rangle$  to  $\langle 100 \rangle$  in the  $a$ - $c$  plane. The  $^{63}\text{Cu}$  NMR frequency is masked by the shaded region for clarity. Thick and thin curves represent the simulated curves for the Al( $a$ ) and Al( $b$ ) sites, respectively.

and  $\nu_Q = 1.58$  MHz ( $V_{ZZ} = 2.92 \times 10^{21}$  V/m $^2$ ) with  $\eta = 0.85$  for CeRhAl<sub>4</sub>Si<sub>2</sub>, similar to the values obtained from fits to the spectra (Fig. 4). Although 4f itinerancy cannot be concluded by this comparison with the experimental values, the calculation captures the basic asymmetry of the EFG and may indicate that the system is

located on the verge of 4f itinerant behavior.

## B. Temperature dependence of $^{27}\text{Al}$ NMR

The Knight shifts and EFG parameters of CeRhAl<sub>4</sub>Si<sub>2</sub> for each temperature are deduced by an exact diagonalization procedure using the data along the  $a$ - and  $c$ -axes in the paramagnetic state. As shown in Fig. 5(a), with decreasing temperature,  $K_c$  increases but  $K_a$  and  $K_b$  decrease slightly. In general, the Knight shift reflects the local magnetic susceptibility at the nuclear site, i.e.,  $K_i(T) - K_{0,i} = A_i \chi_i(T) + A_{0,i} \chi_{0,i}$  ( $i = a, b, c$ ), where  $A_i$  is the transferred hyperfine coupling constant,  $K_{0,i}$  and  $\chi_0$  are the mean temperature-independent terms for the Knight shift and susceptibility, and  $A_{0,i}$  is a coupling constant between the temperature-independent terms, respectively. As shown in Fig. 6, the Knight shifts  $K_i$  versus magnetic susceptibility  $\chi_i$  are plotted with temperature as an implicit parameter. Because the traces are linear, the slopes of the  $K$ - $\chi$  plots yield the transferred hyperfine coupling constants  $A_i$ :  $A_a = -0.6 \pm 0.1$  kOe/ $\mu_B$ ,  $A_b = -0.73 \pm 0.05$  kOe/ $\mu_B$ , and  $A_c = 1.35 \pm 0.01$  kOe/ $\mu_B$ . The values and anisotropy of the Knight shift for  $^{27}\text{Al}$  NMR in CeRhAl<sub>4</sub>Si<sub>2</sub> are similar to those for the related tetragonal compound CeRu<sub>2</sub>Al<sub>2</sub>B, which shows successive magnetic transitions from antiferromagnetism at  $T_N = 14.3$  K to ferromagnetism at  $T_C = 13$  K.<sup>11-13</sup> The magnitudes of transferred dipolar couplings from the 4f moments are estimated to be  $\sim 0.5$  kOe/ $\mu_B$  along the

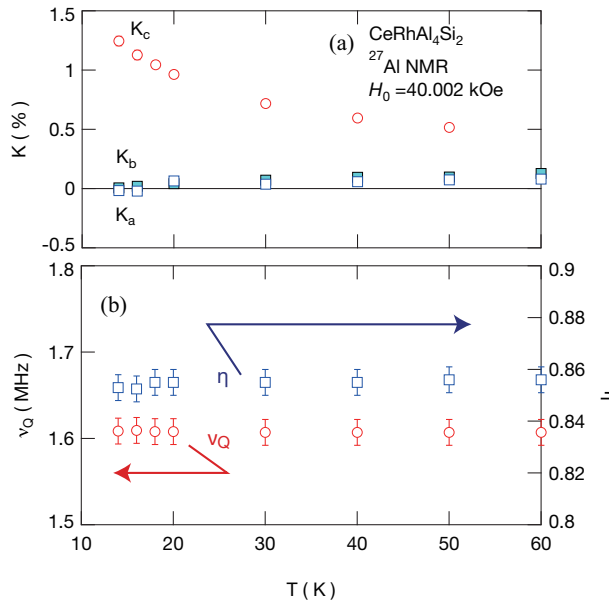


FIG. 5. (Color online) (a) Temperature dependence of the Knight shifts  $K_a$ ,  $K_b$ , and  $K_c$  for  $^{27}\text{Al}$  NMR in  $\text{CeRhAl}_4\text{Si}_2$ . (b) Temperature dependence of the EFG parameters  $\nu_Q$  and  $\eta$  on the Al sites in  $\text{CeRhAl}_4\text{Si}_2$ .

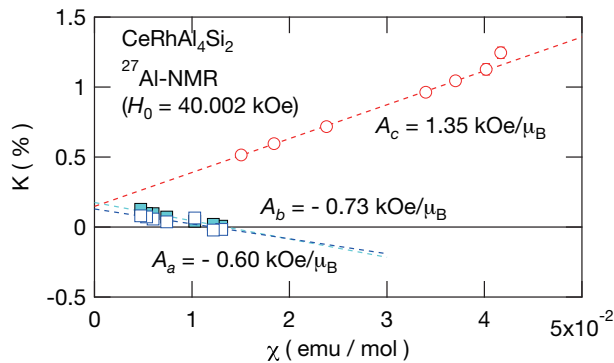


FIG. 6. (Color online)  $K_i$ - $\chi_i$  ( $i = a, b, c$ ) plots with temperature as an implicit parameter for  $^{27}\text{Al}$  NMR in  $\text{CeRhAl}_4\text{Si}_2$ .

$c$ -axis and  $\sim 0.1 \text{ kOe}/\mu_B$  along the  $a$ -axis in  $\text{CeRhAl}_4\text{Si}_2$ . The somewhat larger hyperfine coupling constants could originate from the on-site spin dipolar interaction with the local spin density at the Al  $3p$  orbital in addition to the Fermi contact hyperfine interaction of Al  $3s$  spins. It is noted that the local spin density at Al sites is also transferred from the  $f$  moments via RKKY-type oscillations. In  $\text{CeRhAl}_4\text{Si}_2$ , if  $\chi(T)$  above 250 K is fit to a modified Curie-Weiss function with a temperature independent term, the value of  $\chi_0$  is estimated to be of order  $10^{-4}$  emu/mol, i.e.,  $\chi_0$  is very small. Therefore, the intercepts in the  $K$ - $\chi$  plots, which are small ( $\sim 0.1\%$ ) and are isotropic, correspond roughly to the  $K_{0,i}$  values, and the Knight shifts  $K_i(T)$  are almost completely due to the  $4f$  electron (pseudo-)spin-dependent term. Furthermore,

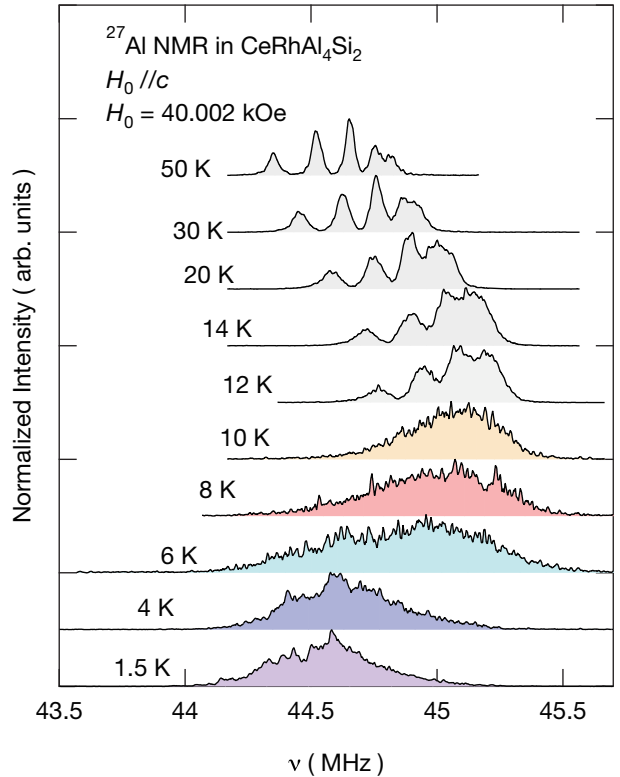


FIG. 7. (Color online) Temperature dependence of the  $^{27}\text{Al}$  NMR spectrum for  $H_0 = 40.002 \text{ kOe}$  along the  $c$ -axis at  $T = 50, 30, 20, 14, 12, 10, 8, 6, 4, 1.5 \text{ K}$ . The respective spectral intensity is normalized by the maximal peak height. These data have been taken with the Ag-coil.

$K_c(T) \gg K_b(T)$  or  $K_a(T)$  indicates an *Ising*-anisotropy of the  $4f$  moments in the paramagnetic state as a consequence of the CEFs. On the other hand,  $\nu_Q$  and  $\eta$  are nearly temperature independent. This indicates that the EFG on the Al sites is nearly constant in this temperature range.

Figures 7 and 8 show the temperature dependence of the  $^{27}\text{Al}$  NMR spectra at  $H_0 = 40.002 \text{ kOe}$  applied along the  $c$ - and  $a$ -axes, respectively. The height of each NMR spectrum is normalized for comparison purposes. According to the  $H$ - $T$  phase diagram by Maurya et al.,<sup>6</sup> the AFM transition temperatures shift down in temperature with magnetic field to  $T_{N1}(H_0) = 11 \text{ K}$  and  $T_{N2}(H_0) = 6.2 \text{ K}$  at  $H_0 = 40 \text{ kOe}$  applied along the  $c$ -axis, whereas  $T_{N1}(H_0) = 13.4 \text{ K}$  and  $T_{N2}(H_0) = 9.2 \text{ K}$  for  $H_0 = 40 \text{ kOe}$  along the  $a$ -axis. Indeed, a remarkable line broadening is observed at  $T = 10 \text{ K}$  in the case of  $H_0 \parallel c$ , as shown in Fig. 7. In the NMR spectrum for  $H_0 \parallel c$  below 10 K, the satellite transitions could no longer be distinguished. As seen in Fig. 7, the spectral center of gravity shifts to higher frequency with decreasing temperature from 50 K, but the interval between transitions does not change. Below  $T_{N1}$ , the center of gravity shifts to lower frequency with decreasing temperature, since the antiferromagnetism reduces the total susceptibility.

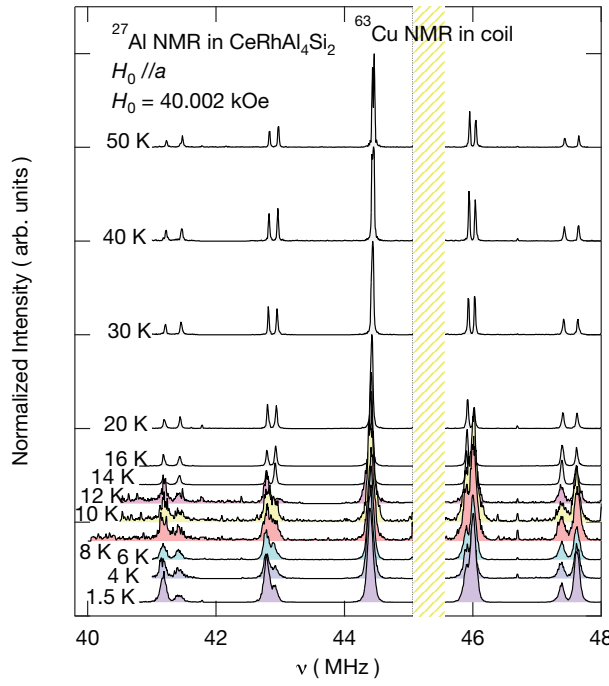


FIG. 8. (Color online) Temperature dependence of the  $^{27}\text{Al}$  NMR spectrum at  $H_0=40.002$  kOe applied along the  $a$ -axis for  $T = 50, 40, 30, 20, 16, 14, 12, 10, 8, 6, 4, 1.5$  K. The respective spectral intensity is normalized by the maximal peak height, and the  $^{63}\text{Cu}$  NMR lines are masked by a hatched rectangle for clarity.

Here, it should be noted that the line width between  $T_{\text{N}1}$  and  $T_{\text{N}2}$  is clearly broader than below  $T_{\text{N}2}$ . On the other hand, the NMR spectrum for  $H_0 \parallel a$  shown in Fig. 8 does not shift with decreasing temperature even below  $T_{\text{N}1}(H_0)$  and  $T_{\text{N}2}(H_0)$ , although the lines broaden very slightly.

### C. $^{27}\text{Al}$ NMR spectral analyses in the antiferromagnetically ordered states

The resonant positions of  $^{27}\text{Al}$  NMR do not change from the PM state to the antiferromagnetically ordered state in the case of  $H_0 \parallel a$ , as magnified for the higher second satellite lines in Fig. 9. In the intermediate AFM state between  $T_{\text{N}1}(H_0) = 12.5$  K and  $T_{\text{N}2}(H_0) = 7.9$  K, which are determined by nuclear relaxation rates as described below, the line widths are broadened only slightly, which may be due to  $c$ -directed internal fields as discussed below. Each peak position labelled as Al( $a$ ) and Al( $b$ ) in Fig. 9 does not shift. On the other hand, as shown in Fig. 7 in the case of  $H_0 \parallel c$ , there is substantial line broadening below  $T_{\text{N}1}(H_0)$  and the center of gravity shifts to lower frequency. This difference of the shift and broadening of spectra in the two different field directions strongly indicates that the transferred internal fields on the Al sites have no projection along the  $a$ -axis in both

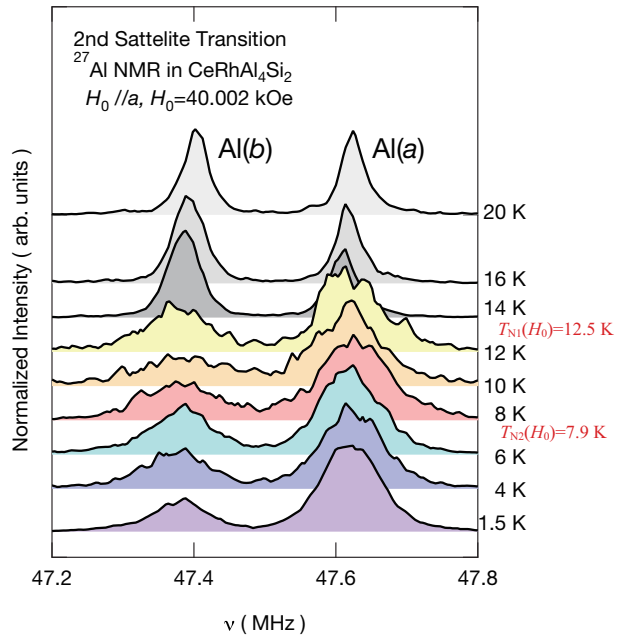


FIG. 9. (Color online) Temperature dependence of the  $^{27}\text{Al}$  NMR spectrum of  $\text{CeRhAl}_4\text{Si}_2$  for the higher second satellite lines in the case of  $H_0 \parallel a$  between 47.2 and 47.8 MHz.

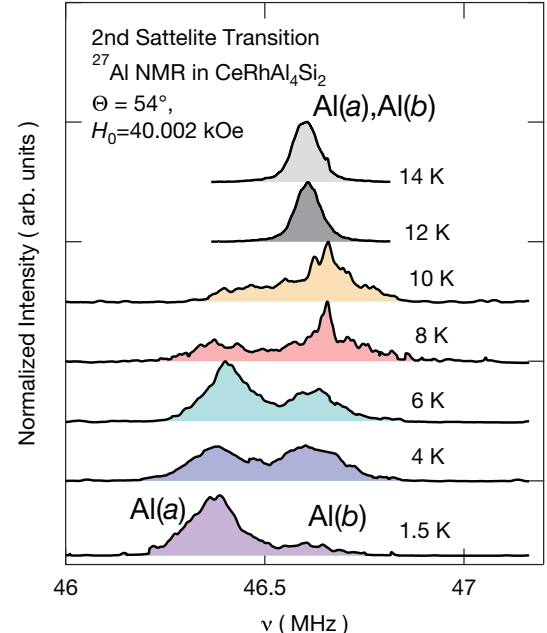


FIG. 10. (Color online) Temperature dependence of the  $^{27}\text{Al}$  NMR spectrum of  $\text{CeRhAl}_4\text{Si}_2$  for the higher second satellite lines for  $\Theta = 54^\circ$ .

AFM states below  $T_{\text{N}1}(H_0)$  and  $T_{\text{N}2}(H_0)$ .

In order to acquire more information relative to the  $c$ -projected transferred field, the NMR spectra with  $H_0$  applied at an angle  $\Theta = 54^\circ$  ( $\Phi = 0$ ) were measured in  $\text{CeRhAl}_4\text{Si}_2$ . As shown in Figs. 3 and 4, the satellite lines of Al( $a$ ) and Al( $b$ ) nearly overlap in this case. Because a

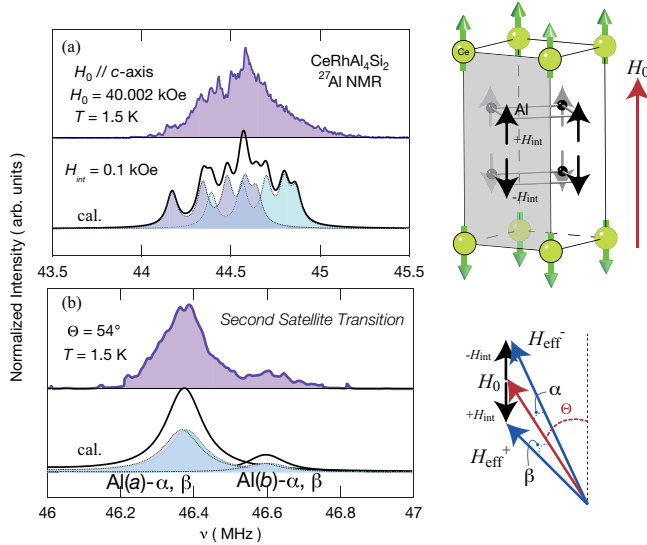


FIG. 11. (Color online) (a) Comparison of the experimental (top) and simulated (bottom) entire Al spectrum for the case of  $H_0 \parallel c$  assuming commensurate AFM Ising order as illustrated in the upper right corner. From the experimental line broadening, the internal fields  $\pm H_{\text{int}}$  at the Al sites are estimated to be  $\sim \pm 0.1$  kOe. (b) same as in (a) for the higher second satellite transition with the external field  $H_0$  at a tilted angle of  $\Theta = 54^\circ$ , assuming the same  $\pm H_{\text{int}}$  along the  $c$ -axis.

clear NMR line broadening is observed at 10 K as shown in Fig. 10,  $T_{\text{N}1}(H_0)$  is considered to be between 12 K and 10 K in this field orientation. To validate these line shapes, so-called  $T_2$  corrections of the intensities have also been applied. It is found that the peak of Al( $b$ ) has a short  $T_2$  at 1.5 K. The line shape at 10 K has a characteristic line shape, reflecting random field orientations, which is discussed below. The line shapes at 10 K and 8 K are similar, but at 6 K, the spectra change markedly indicating that  $T_{\text{N}2}(H_0) \sim 6$  K. At 1.5 K, the spectrum appears to have a double Gaussian shape. Because the splitting of Al( $a$ ) and Al( $b$ ) by the EFG is nearly degenerate upon a tilt of  $\Theta = 54^\circ$ , the apparent line splitting in Fig. 10 for the higher second satellites below  $T_{\text{N}2}(H_0)$ , is due to the development of internal fields on the Al sites.

At the lowest temperature below  $T_{\text{N}2}$ , a commensurate AFM order of Ising moments with  $\mathbf{Q}_2 = (0, 0, 1/2)$  has been confirmed by means of neutron diffraction measurements<sup>7,8</sup>, i.e., the moments with a uniform magnitude of  $\mu_{\text{ord}} \sim 1.1 \mu_B$  on the Ce sites order antiferromagnetically, as schematically shown in the upper right hand of Fig. 11. This magnetic structure is the same as that of the tetragonal heavy fermion antiferromagnets like UPtGa<sub>5</sub> and NpCoGa<sub>5</sub>, for which Ga(2) sites have the same local symmetry as the Al sites in CeRhAl<sub>4</sub>Si<sub>2</sub>. As discussed in our previous reports on these compounds<sup>14,15</sup> in this magnetic structure, since the Al sites have  $C_{2z}$  symmetry, the direction of the internal field  $H_{\text{int}}$  at the Al sites is fixed along the  $c$ -axis.

As shown in Fig. 11(a), when the external field  $H_0$  is applied along the  $c$ -axis, half of the Al sites feels  $H_0 + H_{\text{int}}$ , and the other half feels  $H_0 - H_{\text{int}}$ . Therefore, the two sets of  $^{27}\text{Al}$  NMR should be observed as simulated in Fig. 11(a), although they overlap considerably. From the experimental line width in the case of  $H_0 \parallel c$  at 1.5 K, the  $H_{\text{int}}$  can be estimated to be  $\sim 0.1$  ( $\pm 0.05$ ) kOe at most. This suggests that the hyperfine coupling constant at 1.5 K is drastically reduced from the paramagnetic value of  $A_c = 1.35$  kOe/ $\mu_B$  to  $B_c^{\text{AFM}2} = H_{\text{int}}/\mu_{\text{ord}} \sim 0.09$  kOe/ $\mu_B$ , suggesting a large reduction of local spin densities at the Al sites, in addition to a cancellation of the hyperfine fields at the Al sites by the AFM arrangement of  $4f$  moments. The estimate of  $H_{\text{int}} \sim 0.1$  kOe is supported by reproducing the spectrum for  $\Theta = 54^\circ$  at 1.5 K in Fig. 10 by the simulation as shown in Fig. 11(b). Here, the  $\pm H_{\text{int}}$  produce effective fields  $H_{\text{eff}}^\pm$  at the Al sites, as vector sums illustrated in the lower right hand corner of Fig. 11. As a consequence, the split spectrum of the second satellite transition in Fig. 11(b) can be simulated by half of the Al( $a$ ) sites with tiny  $\theta$ -tilted angles of  $\alpha$  and  $\beta$  and the other half Al( $b$ ) with tiny  $\phi$ -tilted angles, and we estimate  $\alpha + \beta \sim 0.1 - 0.3^\circ$ . Thus, the spectra at 1.5 K below  $T_{\text{N}2}$  can be understood by the commensurate AFM ordering of Ising moments on the Ce sites. We emphasize that the splitting of the Al NMR spectrum is very sensitive to very small tilting angles of  $\Theta$ .

An additional field distribution on the Al sites is required above  $T_{\text{N}2}$  to explain the additional broadening of the line width for  $H_0 \parallel c$  (Fig. 7) and the line shape for  $\Theta = 54^\circ$  (Fig. 10). This comes from the incommensurability of the antiferromagnetism above  $T_{\text{N}2}$ . Again, we note that there is no projection of the internal fields on the Al sites determined from the spectra in the case of  $H_0 \parallel a$  (Fig. 9). Therefore, it is clear that the incommensurability is caused by a SDW modulation of the moments along the  $c$ -axis and not by a spiral rotation of the moments. This is consistent with neutron diffraction measurements.<sup>7,8</sup> Although the propagation vector cannot be determined by NMR spectral analysis because NMR is a local probe on the Al sites, the incommensurability can be verified as follows. In such an incommensurate modulation, the site-to-site internal field on Al sites varies sinusoidally, as illustrated in Fig. 12(b), leading to a histogram of internal fields with a double horn shaped distribution (Fig. 12(c)). By this field distribution, the  $^{27}\text{Al}$  NMR spectrum for  $H_0 \parallel c$  should broaden additionally as shown in Fig. 12(a). Here, to match the experimental line width, the amplitude  $H_{\text{int}}^{\text{max}}$  of the field distribution is set at  $\sim 0.1$  ( $\pm 0.05$ ) kOe. The NMR spectrum with  $\Theta = 54^\circ$  may be reproduced with a sum of two double horn spectra of Al( $a$ ) and Al( $b$ ) sites shown in Fig. 12(d) after the exact diagonalization procedure. If the estimate of  $\mu_{\text{ord}} = 0.65 \mu_B$  from neutron scattering at 10 K is used<sup>8</sup>, the transferred hyperfine coupling constant in the incommensurate ordered phase can be estimated to be  $B_c^{\text{AFM}1} \sim 0.15$  kOe/ $\mu_B$ .  $B_c^{\text{AFM}1}$  becomes a bit larger than the  $B_c^{\text{AFM}2}$  probably due to incomplete

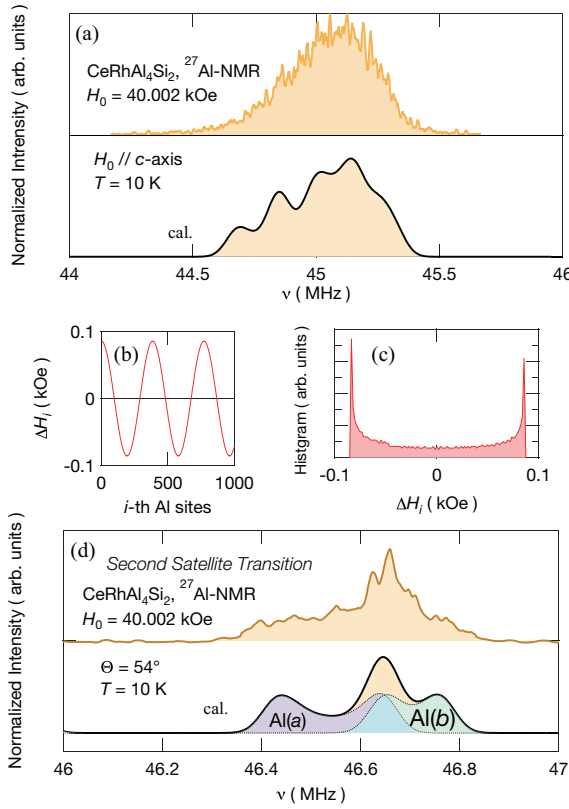


FIG. 12. (Color online) (a) Comparison of the experimental (top) and simulated (bottom) by an SDW model for the <sup>27</sup>Al NMR spectrum for the case of  $H_0 \parallel c$  at 10 K. (b) Assumed oscillation of internal fields on the Al sites. (c) Histogram of the internal fields for the assumed oscillation. (d) same as in (a) for the higher 2nd satellite transition on a tilt of  $\Theta = 54^\circ$  at 10 K.

AFM cancellation of the hyperfine fields. These  $B_c^{\text{AFM1}}$  and  $B_c^{\text{AFM2}}$  are, however, much smaller than the paramagnetic value of  $A_c$ , indicating a large reduction of spin densities at the Al sites. Reductions of both the hyperfine coupling constant and ordered moment indicate the presence of a strong Kondo interaction below  $T_{\text{N1}}$ .

#### D. Spin dynamics in CeRhAl<sub>4</sub>Si<sub>2</sub>

Finally, we discuss the spin dynamics in CeRhAl<sub>4</sub>Si<sub>2</sub>. Figure 13 shows the temperature dependence of nuclear spin-lattice relaxation rate  $1/T_1$  of <sup>27</sup>Al in CeRhAl<sub>4</sub>Si<sub>2</sub> at  $H_0 = 40.002$  kOe for  $H_0 \parallel a, b, c$ . The values are magnetically enhanced from the Korringa rates by conduction electrons, which is usually estimated from the La analog and typically has a small value of  $1/T_1 T$  ranging between 0.01–0.1 (sec K)<sup>-1</sup>. For example,  $1/T_1 T = 0.02$  (sec K)<sup>-1</sup> has been estimated for LaRu<sub>2</sub>Al<sub>2</sub>B.<sup>16</sup>

In general,  $1/T_1$  can be expressed<sup>17</sup> as

$$\frac{1}{T_1} = \frac{k_B T}{(\gamma_e \hbar)^2} \cdot 2(\gamma_N A_\perp)^2 \sum_q f_\perp^2(\mathbf{q}) \frac{\text{Im} \chi_\perp(\mathbf{q}, \omega_0)}{\omega_0}, \quad (3)$$

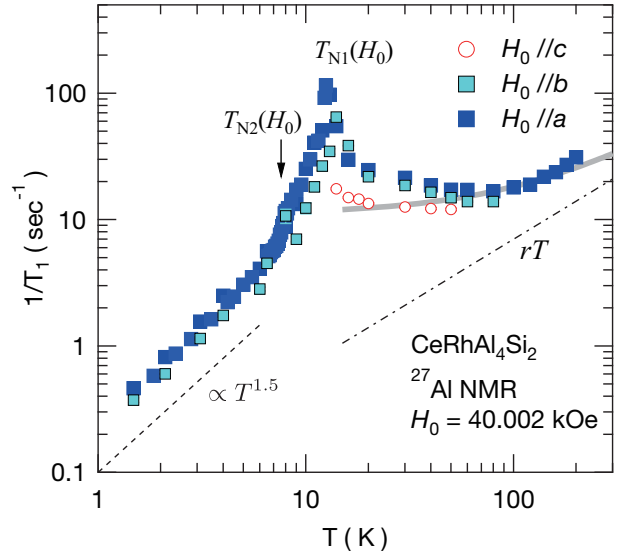


FIG. 13. (Color online) (a) Temperature dependence of the nuclear spin-lattice relaxation rate  $1/T_1$  of <sup>27</sup>Al in CeRhAl<sub>4</sub>Si<sub>2</sub> at  $H_0 = 40.002$  kOe for  $H_0 \parallel a, b, c$ . The thick curve denotes the calculated  $1/T_1$  using the localized 4f model described in the text. The dot-dashed line ( $rT$ ) represents the estimated Korringa rate by conduction electrons. The dotted line is a guide to the eye for a  $T^{1.5}$ -dependence.

where  $\gamma_e$  is the electronic gyromagnetic ratio,  $f_\alpha(\mathbf{q})$  is the hyperfine form factor (taken as unity for simplicity in the following analysis),  $\text{Im} \chi(\mathbf{q}, \omega_0)$  is the imaginary part of the dynamical susceptibility,  $\omega_0$  is the nuclear Larmor frequency and  $\perp$  refers to the component perpendicular to the quantization axis. Thus, the nuclear spin-lattice relaxation rate  $1/T_1$  is driven by low-energy spin-fluctuation densities, and  $1/T_1$  is sensitive to the perpendicular fluctuations in an applied external field.

At a first glance, a peak at  $T_{\text{N1}}(H_0)$  and a point of inflection at  $T_{\text{N2}}(H_0)$  in  $1/T_1$  are observed for Al(a) and Al(b). In the AFM states,  $1/T_1$  decreases rapidly below  $T_{\text{N1}}(H_0)$  and  $T_{\text{N2}}(H_0)$ . Below  $\sim 4$  K,  $1/T_1$  decreases as temperature decreases and follows a power law of  $T^{1.5}$ . In localized antiferromagnets,  $1/T_1$  is governed at the lowest temperatures by a multimagnon process of the spin wave excitations and is expected to vary as  $T^2 \exp(-E_G/T)$  or  $T^5$  when the temperature becomes lower than that corresponding to the spin wave gap  $E_G$ .<sup>18</sup> In this sense, the characteristic power law  $T^{1.5}$  may suggest that the relaxation mechanism cannot be explained by such a magnon process. Additional terms due to the strong *Ising* anisotropy, by anisotropic exchange couplings on the quasi-2D lattice, or by intermingled nature of itinerant and localized Ce moments, need to be considered in these AFM states.

At higher temperatures above  $T_K$ ,  $1/T_1$  may be described by excitations from the localized 4f electrons in CeRhAl<sub>4</sub>Si<sub>2</sub> with a small Korringa rate by conduction electrons. Using the proposed CEF scheme,<sup>6</sup> this contribution may be calculated from the following

formula<sup>19–22</sup>,

$$\left(\frac{1}{T_1}\right)_{\text{CEF}} = \frac{2\gamma_N^2 |(A/z')^2|}{\omega_{\text{ex}}} \sum_j \frac{|\langle J_z \rangle_j|^2 \exp(-E_j)/k_B T}{Z}, \quad (4)$$

with a characteristic exchange angular frequency  $\omega_{\text{ex}}$ , where  $z'$  and  $z$  are the numbers of nearest neighboring Ce ions from the ligand sites and Ce sites, respectively, and  $\langle J_z \rangle_j$  is the expectation value of  $J_z$  for the  $j$ -th CEF eigen state and  $Z$  is the single-ion partition function.  $\omega_{\text{ex}}$  may be expressed as  $(\sqrt{2z}/\sqrt{3}\hbar)I_{\text{ex}}p_{\text{eff}}$  with an exchange interaction  $I_{\text{ex}}$  and an effective moment  $p_{\text{eff}}$  of Ce ions.<sup>23</sup> The thick curve in Fig. 13 is obtained by the sum of  $(1/T_1)_{\text{CEF}} + rT$  with  $\omega_{\text{ex}}$  assuming  $p_{\text{eff}} = 2.54 \mu_B$ ,  $I_{\text{ex}} \sim 14 \text{ K}$  and a small Korringa rate  $r$  of  $0.07 (\text{sec K})^{-1}$  due to conduction electrons, which can reproduce the temperature dependence and the values of  $1/T_1$  above  $\sim 30 \text{ K}$ . Below  $\sim 30 \text{ K}$ , critical slowing-down of spin fluctuations causes the increase of  $1/T_1$  toward  $T_{\text{N}1}(H_0)$ . Thus, at temperatures above  $\sim 30 \text{ K}$ , the  $4f$  electrons may be regarded from the spin dynamics as fully localized, so the previous estimate of  $T_K \sim T_{\text{N}1}(0)$  appears to be reasonable.<sup>5</sup> Interestingly, the anisotropy of  $1/T_1$  becomes rather prominent below  $\sim 30 \text{ K}$ . The  $c$  component of  $1/T_1$  is minimal and the  $a$  component is maximal, reflecting an *Ising*-type anisotropy in the spin dynamics

as well.

#### IV. SUMMARY

We have performed  $^{27}\text{Al}$  NMR measurements on the Kondo lattice compound  $\text{CeRhAl}_4\text{Si}_2$ . In the paramagnetic and antiferromagnetically ordered states, an *Ising*-type anisotropy along the  $c$ -axis governs the static and dynamic magnetism. The analysis of  $^{27}\text{Al}$  NMR spectra indicates an incommensurate AFM state between  $T_{\text{N}1}$  and  $T_{\text{N}2}$  and commensurate AFM order below  $T_{\text{N}2}$ . Because the incommensurability may come from nesting of the Fermi surface,<sup>5,6</sup> further study of the Fermi surface is warranted. Spin dynamics in  $\text{CeRhAl}_4\text{Si}_2$  suggests that this material is on the verge of  $4f$  itinerancy and provides a basis to understand this new series of  $\text{CeTAl}_4\text{Si}_2$  ( $T=\text{Rh, Ir, Pt}$ ) compounds.

#### ACKNOWLEDGMENTS

We thank J. Lawrence for valuable discussions. Work at Los Alamos National Laboratory was performed under the auspices of the US Department of Energy, Office of Basic Energy Sciences, Division of Materials Sciences and Engineering. Work in Japan was partly supported by the Reime Research Program of JAEA.

\* sakai.hironori@jaea.go.jp

† Present address: Materials Science Division, Argonne National Laboratory, Argonne, Illinois 60439, USA.

<sup>1</sup> W. Bao, P. G. Pagliuso, J. L. Sarrao, J. D. Thompson, Z. Fisk, J. W. Lynn, and R. W. Erwin, *Phys. Rev. B* **62**, R14621 (2000).

<sup>2</sup> O. Stockert, E. Faulhaber, G. Zwicknagl, N. Stüber, H. S. Jeevan, M. Deppe, R. Borth, R. Küchler, M. Loewenhaupt, C. Geibel, and F. Steglich, *Phys. Rev. Lett.* **92**, 136401 (2004).

<sup>3</sup> H. Hegger, C. Petrovic, E. G. Moshopoulou, M. F. Hundley, J. L. Sarrao, Z. Fisk, and J. D. Thompson, *Phys. Rev. Lett.* **84**, 4986 (2000).

<sup>4</sup> F. Steglich, J. Aarts, C. D. Bredl, W. Lieke, D. Meschede, W. Franz, and H. Schäfer, *Phys. Rev. Lett.* **43**, 1892 (1979).

<sup>5</sup> N. J. Ghimire, F. Ronning, D. J. Williams, B. L. Scott, Y. Luo, J. D. Thompson, and E. D. Bauer, *J. Phys. :Condens. Matter* **27**, 025601 (2015).

<sup>6</sup> A. Maurya, R. Kulkarni, A. Thamizhavel, D. Paudyal, and S. K. Dhar, *cond-mat* , arXiv:1501.00250 (2015).

<sup>7</sup> N. J. Ghimire, S. Calder, M. Janoschek, and E. D. Bauer, *J. Phys. :Condens. Matter* **27**, 245603 (2015).

<sup>8</sup> J. Gunasekera, L. Harriger, A. Dahal, A. Maurya, T. Heitmann, S. Disseler, A. Thamizhavel, S. Dhar, and D. K. Singh, *cond-mat* , arXiv:1509.02092 (2015).

<sup>9</sup> J. P. Perdew, K. Burke, and M. Ernzerhof, *Phys. Rev. Lett.* **77**, 3865 (1996).

<sup>10</sup> P. Blaha, K. Schwarz, G. Madsen, D. Kvasnicka, and J. Luitz, *An Augmented Plane Wave + Local Orbitals Program for Calculating Crystal Properties* (K. Schwartz, Techn. Universität Wien, Austria, 2001).

<sup>11</sup> R. E. Baumbach, X. Lu, F. Ronning, J. D. Thompson, and E. D. Bauer, *J. Phys. :Condens. Matter* **24**, 325601 (2012).

<sup>12</sup> E. Matsuoka, Y. Tomiyama, H. Sugawara, T. Sakurai, and H. Ohta, *J. Phys. Soc. Jpn.* **81**, 043704 (2012).

<sup>13</sup> H. Matsuno, H. Nohara, H. Kotegawa, E. Matsuoka, Y. Tomiyama, H. Sugawara, H. Harima, and H. Tou, *J. Phys. Soc. Jpn.* **81**, 073705 (2012).

<sup>14</sup> H. Kato, H. Sakai, S. Kambe, R. E. Walstedt, Y. Tokiwa, and Y. Ōnuki, *Acta Physica Polonica B* **34**, 1063 (2003).

<sup>15</sup> H. Sakai, S. Kambe, Y. Tokunaga, T. Fujimoto, R. E. Walstedt, H. Yusuoka, D. Aoki, Y. Homma, E. Yamamoto, A. Nakamura, Y. Shiokawa, and Y. Ōnuki, *Phys. Rev. B* **76**, 024410 (14) (2007).

<sup>16</sup> H. Matsuno, H. Kotegawa, E. Matsuoka, Y. Tomiyama, H. Sugawara, and H. Tou, *J. Phys. Soc. Jpn.* **83**, 103709 (2014).

<sup>17</sup> T. Moriya, *J. Phys. Soc. Jpn.* **18**, 516 (1963).

<sup>18</sup> D. Beeman and P. Pincus, *Phys. Rev.* **166**, 359 (1968).

<sup>19</sup> H. Tanida, S. Takagi, H. S. Suzuki, I. Satoh, and T. Komatsubara, *J. Phys. Soc. Jpn.* **75**, 074721 (2006).

<sup>20</sup> T. Moriya and Y. Obata, *J. Phys. Soc. Jpn.* **13**, 1333 (1958).

<sup>21</sup> K. Sugawara, *J. Phys. Soc. Jpn.* **42**, 1154 (1977).

<sup>22</sup> K. Sugawara, *J. Phys. Soc. Jpn.* **42**, 1161 (1977).

<sup>23</sup> T. Moriya, Prog. Theor. Phys. **16**, 23,641 (1956).